Article

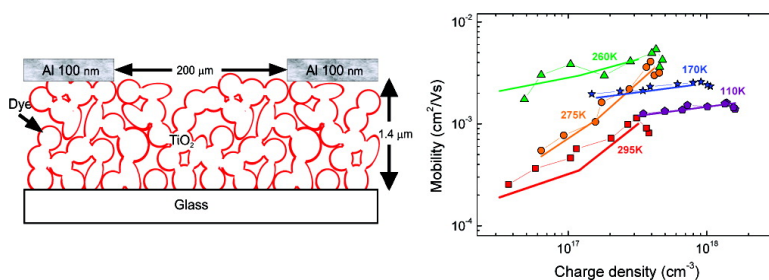# Electron Transport and Recombination in Dye-Sensitized Mesoporous TiO Probed by Photoinduced Charge-Conductivity Modulation Spectroscopy with Monte Carlo Modeling

Annamaria Petrozza, Chris Groves, and Henry J. Snaith

More About This Article

Additional resources and features associated with this article are available within the HTML version:

- Supporting Information
- Access to high resolution figures
- Links to articles and content related to this article
- Copyright permission to reproduce figures and/or text from this article

View the Full Text HTML

Electron Transport and Recombination in Dye-Sensitized Mesoporous TiO₂ Probed by Photoinduced Charge-Conductivity Modulation Spectroscopy with Monte Carlo Modeling

Annamaria Petrozza,† Chris Groves,† and Henry J. Snaith*,‡

Cavendish Laboratory, Department of Physics, University of Cambridge, J.J. Thomson Avenue, Cambridge CB30HE, U.K., and Clarendon Laboratory, Department of Physics, University of Oxford, Parks Road, Oxford OX1 3PU, U.K.

Received March 21, 2008; E-mail: h.snaith1@physics.ox.ac.uk

Abstract: We present a combined experimental and theoretical investigation into the charge transport and recombination in dye-sensitized mesoporous TiO₂. We electronically probe the photoinduced change in conductivity through in-plane devices while simultaneously optically probing signatures of the charge species. Our quasi-continuous wave technique allows us to build data sets of electron mobility and recombination versus charge density over a wide temperature range. We observe that the charge density dependence of mobility in TiO₂ is strong at high temperatures and gradually reduces with reducing temperature, to an extent where at temperatures below 260 K the mobility is almost independent of charge density. The mobility first increases and then decreases with reducing temperature at any given charge density. These observed trends are surprising and consistent with the multiple-trapping model for charge transport only if the trap density-of-states (DoS) is allowed to become less deep and narrower as the temperature reduces. Our recombination measurements and simulations over a broad range of charge density and temperature are also consistent with the above-mentioned varying DoS function when the recombination rate constant is allowed to increase with temperature, itself consistent with a thermally activated charge-transfer process. Further to using the Monte Carlo simulations to model the experimental data, we use the simulations to aid our understanding of the limiting factors to charge transport and recombination. According to our model, we find that the charge recombination is mainly governed by the recombination reaction rate constant and the charge density dependence is mainly a result of the bimolecular nature of the recombination process. The implication to future material design is that if the mobility can be enhanced without increasing the charge density in the film, for instance by reducing the average trap depth, then this will not be at the sacrifice of comparably enhanced recombination and it will greatly increase the charge carrier diffusion lengths in dye-sensitized or mesoscopic solar cells.

Introduction

Mesoporous materials are of increasing technological interest, specifically in energy-related fields such as batteries, fuel cells, and photovoltaics, where an extremely large internal surface between dissimilar components is required. Unlike conventional bulk crystals, large densities of surface states and defect sites are ubiquitous with mesoporous materials and usually determine the macroscopic properties of the material, such as mobility and surface reactivity. However, despite the performance-limiting aspects of defect states, mesoporous TiO₂ has recently received considerable attention due to its excellent performance when incorporated into photoelectrochemical dye-sensitized solar cells (DSCs)[1] and its potential usage in batteries.[2,3] In brief, the most efficiently operating dye-sensitized solar cells are composed of a mesoporous TiO₂ metal-oxide electrode fabricated from sintered nanoparticles (∼20 nm in diameter, 60% porosity) coated upon transparent conducting glass (fluorine-doped tin oxide (SnO₂:F(FTO))). The porosity of the film delivers an approximate 100-fold enhancement in surface area per micrometer thickness when compared to that of a flat film. The mesoporous film is sensitized with a monolayer of dye, filled with an iodide/triiodide-based electrolyte, and capped with a platinum counter electrode. Light absorption takes place in the dye molecules, with subsequent electron transfer from the excited states of the dye to the conduction band of the TiO₂. The porosity and roughness of the film primarily accounts for the high performance of DSCs, since it endows the film with a large surface area which enables a high degree of dye loading. The inclusion of larger-scale particles (over 100 nm in diameter) can also efficiently scatter the light into the plane of the device and thus increase light absorption. Electron transport to the anode occurs via diffusion of electrons through the disordered network of TiO₂ nanoparticles. The oxidized dye molecules are regenerated by the iodide redox couple with the positive charge

† University of Cambridge.
‡ University of Oxford.
(1) O'Regan, B.; Grätzel, M. *Nature* **1991**, *353*, 737.
(2) Huang, S. Y.; Kavan, L.; Exnar, I.; Grätzel, M. *J. Electrochem. Soc.* **1995**, *142*, L142.
(3) Croce, F.; Appetecchi, G. B.; Persi, L.; Scrosati, B. *Nature* **1998**, *394*, 456.

being transported through the electrolyte (triiodide species) to the platinum counter electrode.

Unraveling the transport and recombination mechanisms in dye-sensitized solar cells has not been straightforward, and to date there exist many contradictory reports where the experimentally observed trends do not appear to match those theoretically predicted. The most broadly accepted description of charge transport in TiO₂ is the multiple-trapping (MT) model, in which electrons are mobile only when they detrap to a high-energy conduction band, or mobility edge. Hence, in the MT model, the mobility is limited by the trap density and the rate of detrapping of charges to the mobile region. In order to verify a theoretical model, it is clearly essential that, when varying all parameters, the observed response is as expected. Temperature is a very useful tool in this respect; however, this specific parameter has led to considerable disagreement on the topic of charge transport and recombination in DSCs.[4−7] One of the difficulties in deriving the charge transport characteristics, or indeed the recombination characteristics, directly from measurements on these solar cells is that most of the rates governing all the processes have some temperature dependence.[6] Therefore, only varying one parameter with temperature, and more specifically keeping the charge density in the device constant with changing temperature, is highly challenging. The presence of an electrolyte and a temperature dependence of the surface potential and ionic adsorption to the TiO₂ surface further complicate the situation.

Here we present a new technique for measuring the electron transport and recombination in dye-sensitized mesoporous materials in which the charge density is probed directly by quasi-continuous wave (cw) optical absorption measurements while simultaneously electronically measuring the conductivity through in-plane devices. This enables the charge carrier mobility to be extracted while varying and knowing the charge density over a broad range of temperatures. We observe an unexpected trend of mobility with temperature. However, our results are consistent with the MT model for charge transport if the trap density-of-states (DoS) is allowed to become less deep and narrower as the temperature reduces. Our recombination measurements and simulations over a broad range of charge density and temperature are also consistent with the above-mentioned varying DoS function when the recombination rate constant is allowed to increase with temperature, itself consistent with a thermally activated charge-transfer process. Our study goes some way to confirming the validity of the MT model for charge transport and its influence upon recombination when applied to dye-sensitized mesoporous systems.

Experimental Technique

Device Fabrication. We measure the conductivity in TiO₂ using in-plane "electron-only" devices, the structure of which is shown schematically in Figure 1a. A 1.4 μm thick layer of mesoporous TiO₂ with ~60% porosity and comprising of nanoparticles of 20 nm in diameter is deposited upon a transparent glass substrate as described elsewhere.[8] These films are sintered at 500 °C and cooled, and interdigitated in-plane aluminum contacts are thermally evapo-
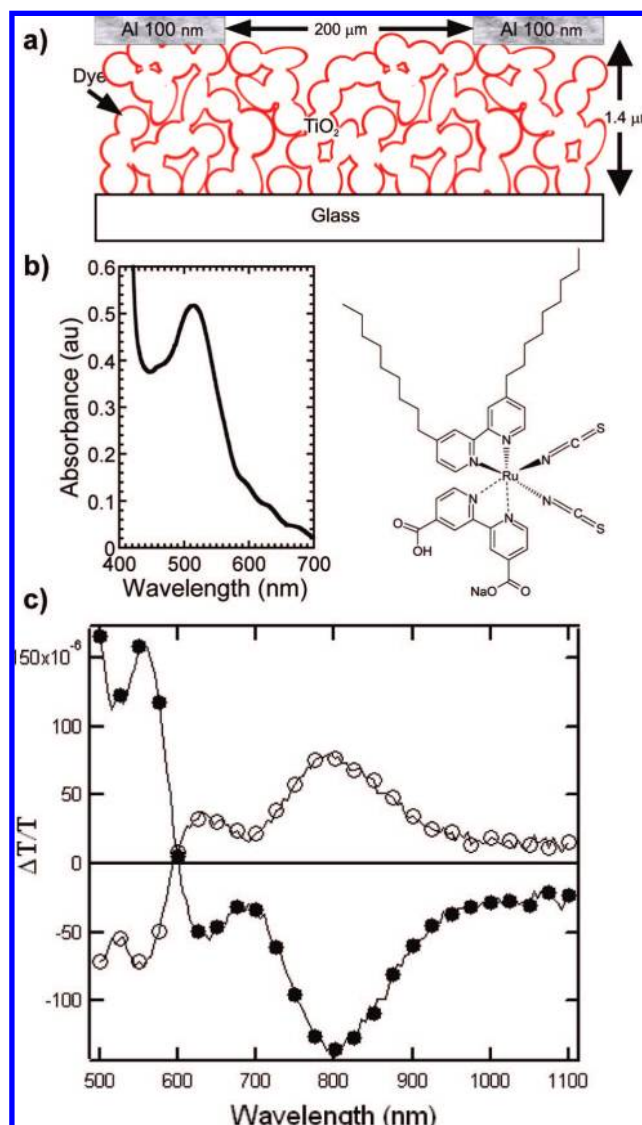

Figure 1. (a) Schematic illustration of the electron-only device structure used in this study. The mesoporous film is about 1.4 μm thick between a glass substrate and the aluminum interdigitated electrodes, which creates a 200 μm wide and 4 cm long channel. (b) UV−vis absorption spectra for a 2 μm thick film of mesoporous TiO₂ coated with a monolayer of Z907 ruthenium complex, the chemical structure of which is shown to the right. The molar extinction coefficient measured in solution at the 514 nm peak is approximately 13 000 cm⁻¹ M⁻¹, and that at 560 nm (where the bleaching is measured) is approximately 7000 cm⁻¹ M⁻¹. (c) Photoinduced absorption spectrum from a 1.4 μm thick mesoporous TiO₂ film sensitized with the ruthenium complex Z907. It is pumped at 488 nm with an intensity of 128 mW cm⁻² and a modulation frequency of 200 Hz. The open circles correspond to the signal out-of-phase with the pump light, and the filled circles correspond to the in-phase signal.

rated on top of them under high vacuum in order to create a $w = 200$ μm channel with a total channel length of $L = 4$ cm ($L/w = 200$). After electrode deposition, the films are immersed in a 0.5 mM solution (1:1 v/v acetonitrile:*tert*-butanol) of ruthenium complex dye, termed Z907, overnight.[9] The UV−vis absorption spectrum for the dye along with the chemical structure is shown in Figure 1b.

Photoinduced Charge-Conductivity Modulation spectroscopy. The conductivity of a material, σ, is related to the density of charges, n, and their mobility, μ, through the relationship

(4) Boschloo, G.; Hagfeldt, A. *J. Phys. Chem. B* **2005**, *109*, 12093.
(5) Peter, L. M.; Walker, A. B.; Boschloo, G.; Hagfeldt, A. *J. Phys. Chem. B* **2006**, *110*, 13694.
(6) O'Regan, B.; Durrent, J. R. *J. Phys. Chem. B* **2006**, *110*, 8544.
(7) Kopidakis, N.; Benkstein, K. D.; van de Lagemaat, J.; Frank, A. J.; Yuan, Q.; Schiff, E. A. *Phys. Rev. B* **2006**, *73*, 045326.
(8) Snaith, H. J.; Schmidt-Mende, L.; Chiesa, M.; Gratzel, M. *Phys. Rev. B* **2006**, *74*, 045306.
(9) Wang, P.; Zakeeruddin, S. M.; Moser, J. E.; Nazeeruddin, M. K.; Sekiguchi, T.; Gratzel, M. *Nat. Mater.* **2003**, *2*, 402.

$$\sigma = \mu n e \qquad (1)$$

where e is the electron charge. In this study, two techniques have been combined which simultaneously measure the photoconductivity (PC) and charge density under illumination in order to extract the electron mobility under known conditions. The charge density was obtained through photoinduced absorption (PIA) spectroscopy, which is a quasi-cw pump−probe technique sensitive to the absorption of photogenerated long-lived species (from microseconds to milliseconds). The setup used is described elswhere.[10] Pump excitation was provided by an argon ion laser tuned to 488 nm, the intensity of which was attenuated by a continuous optical density filter wheel. The monochromatic probe used was generated from a 100 W halogen lamp. The changes in transmission under photoexcitation, detected by a lock-in amplifier referenced to the modulation frequency, were normalized to the unmodulated transmission for every wavelength ($\Delta T/T$). All samples were measured in a continuous-flow helium cryostat under a low-pressure helium atmosphere.

Pump excitation was absorbed by the dye, whereupon there was ultrafast electron injection from the photoexcited dye to the TiO_2. Because of the extremely efficient electron-transfer process, we consider that each oxidized dye species corresponds to an electron injected into the TiO_2, which can be free or trapped. The density of electrons in the TiO_2 was therefore monitored by probing the photobleaching signal of the dye. The density of bleached species is given by

$$n_{dye} = \frac{N_a \Delta OD}{1000 \varepsilon d} \qquad (2)$$

where N_a is Avogadro's number, ΔOD is the change in the optical density, obtained through $\Delta OD = -\log_{10}(1 + \Delta T/T)$, $\Delta T/T$ is the fractional change in transmission directly measured by the PIA experiment at 560 nm, d the film thickness, and ε is the extinction coefficient at the probed wavelength.

To measure the conductivity, the device was biased by a 3.2 V battery source and connected in series with a small resistor. The photoconductivity was measured simultaneously with the PIA signal through a digital oscilloscope probing across the series resistor. The oscilloscope was triggered at the same frequency used to modulate the excitation source. The conductivity is given by $\sigma = J/E$, where J is the current density in the channel and E is the electric field. Therefore, knowing the geometry of the device one can write

$$\Delta \sigma = \frac{IL}{Vwt} = \frac{\Delta V_{OS}L}{rVwt} \qquad (3)$$

where $\Delta \sigma$ is the change in conductivity under illumination, I is the photocurrent, L is the channel length, w is the channel width, t is the film thickness, ΔV_{OS} is the change in voltage read on the oscilloscope due to the photoexcitation of the device, and r is the parallel combination of the internal resistance of the oscilloscope (normally 1 MΩ) and the series resistor used to read the photovoltage, ranging from 1 to 30 kΩ depending on the magnitude of the signal, and V is the voltage applied by the external battery (3.2 V). The photoinduced voltage drop across the series resistor was always kept to below 20 mV. For the measured change in resistance between the electrodes to truly reflect the change in conductivity in the channel, there must be negligible contact resistance and the current must not be limited by space-charge effects. Aluminum makes a very good electronic contact to TiO_2 with negligible contact resistance. This is illustrated by the use of TiO_2 as an electron collection layer between an organic semiconductor and aluminum electrodes in organic solar cells, where the overall series resistance of the cells is only 10 Ω cm^{-2}, putting an upper limit on the contact resistance.[11] The channel resistance in our devices ranges from MΩs

to GΩs depending on light intensity. The channel resistance clearly dominates since the channel is 4 cm long and there is a metal contact area of the order of 0.1 cm^2. For a field-independent mobility, space-charge-limited current (SCLC) follows $J_{scl} = \frac{9}{8} \varepsilon_0 \varepsilon_r \mu_n V^2/w^3$, where ε_r is the dielectric constant, μ_n is the electron mobility, and w is the channel width or film thickness. First, we observe linear JV curves inconsistent with SCLC. Second, in this system there is a large quantity of ions and counterions introduced from the dye molecules and an equal proportion of photogenerated electrons and holes throughout the film. This will all amount to a large degree of charge compensation, minimizing space-charge effects. Furthermore, if we calculate the SCLC we expect from our devices under the conditions measured, using $\varepsilon_r = 100$ and $\mu_n = 10^{-4}$ cm^2/V·s for mesoporous TiO_2, we get $J_{scl} \approx 10^{-5}$ A/m^2. Our measured current densities range from 0.1 to 1000 A/m^2. This demonstrates that the conductivity arises from conductive species within the channel, in this case photogenerated charge carriers, and not from SCLC. We note here that the system we are measuring is dyed, mesoporous TiO_2 and in this case in a helium atmosphere. The conductivity in TiO_2 is strongly influenced by its surrounding medium, including the presence or absence of oxygen, water, and ionic species.[12] We measure in a water-free, oxygen-free atmosphere so any temperature-dependent changes associated with adsorption or desorption of these molecules should be negligible. Furthermore, we are measuring the photoconductivity, which is orders of magnitude higher than the residual dark conductivity, suggesting that changes to the latter should not significantly affect the derived results. We also note that all the reported trends are directly reversible in both temperature and charge density variations. We do note however, though we have measured a component part of the dye-sensitized solar cell, there are expected to be considerable differences as compared to an electrolyte-filled medium. Most importantly here, if a temperature dependence of the density of trap states predominantly arises from a Coulomb term, then this is likely to alter when surrounded by ionic species.

The electron mobility in the TiO_2 films can be determined by the ratio of photoconductivity to the total charge density (i.e., including free and trapped charges). In this way we measure the average mobility for an average quasi-steady-state charge density. Since the electrons are continually injected from photoexcited dye and lost to recombination, our current measurements do implicitly include information about the recombination rate. One might therefore ask whether our mobility data are sensitive to changes in the recombination rate when, for example, the temperature is changed. However, under steady-state conditions, every charge pair which recombine are replaced with a photoinjected charge pair throughout the channel, and hence on average the recombination does not contribute to the current. We note that the conductivity arises predominantly from electrons in the TiO_2, and we consider the holes on the dye to be relatively immobile; hence we are measuring an electron-only current, and again a recombination current should not be contributing, contrary to what would be the case in a photovoltaic system with mobile electrons and holes. Changes in the recombination rate do alter the quasi-steady-state population of electrons, but since we measure the population of electrons directly, our mobility data account for this. Since the population of electrons contributing to the photoconductivity is known, the measured mobility, and its physical meaning (i.e., the ratio of the drift velocity of an ensemble of carriers to the electric field), should be the same as that of other, more standard techniques such as time-of-flight and space-charge-limited diodes.

The photogenerated charge density is estimated from the sum of the in-phase and out-of-phase photoinduced bleaching signal. We measure the photoinduced change in conductivity by taking the difference of the maximum and the minimum of the PC trace during the modulation cycle. However, taking such an approach

(10) Ginger, D. S.; Greenham, N. C. *Phys. Rev. B* **1999**, *59*, 10622.
(11) Kim, J. Y.; Kim, S. H.; Lee, H. H.; Lee, K.; Ma, W.; Gong, X.; Heeger, A. J. *Adv. Mater.* **2006**, *18*, 572.

(12) Kytin, V.; Dittrich, T.; Bisquert, J.; Lebedev, E. A.; Koch, F. *Phys. Rev. B* **2003**, *68*, 195308.

neglects the species that are longer lived than the modulation cycle. Ideally we would modulate infinitely slowly to minimize this problem, but noise puts a lower limit to the modulation frequency of 23 Hz. We therefore estimated the background charge density using another method. If we assume that the charge density is approximately linearly dependent upon the conductivity, this in turn allows us to estimate the background charge density from the background conductivity, which is simply the minimum of the PC trace during the off cycle of the excitation. This background contribution is added to the photoexcited charge density estimated from the PIA measurements to give a close approximation of the total charge density in the film. We make this extra effort to quantify the charge density since we wish to safeguard against a large background charge density giving an apparent enhancement in photoconductivity. However, in practice the measured photoconductivity is in most cases much larger than the dark conductivity, and so the correction is small. Indeed, in the most extreme cases this first-order approximation alters the absolute value of mobility by a factor of ∼2 and makes no difference to the trends observed, as will be discussed later. We term this combined technique as "photoinduced charge-conductivity modulation spectroscopy".

Experimental Results

Electron Transport. In Figure 1c, the in-phase and out-of-phase PIA spectra are shown for a 1.4 μm thick film of mesoporous TiO₂ sensitized with the ruthenium complex Z907. At short wavelengths (500 nm < λ < 600 nm) the in-phase PIA signal is positive; this band is assigned to $S_0 \rightarrow S_1$ photobleaching of the dye species, as a comparison with its UV−vis absorption spectrum can confirm. At longer wavelengths the signal becomes negative due to the absorbance of photoinduced species; the strongest band, peaking at $\lambda = 800$ nm, has been assigned to the oxidized species in the dye, which also appears around $\lambda = 630$ nm,[13] and a small contribution from of the electron absorption in TiO₂ can be observed in the infrared spectral region.[14]

Figure 2a shows the PIA signal at $\lambda = 560$ nm as a function of the excitation intensity. From these data one can calculate the effective density of charges (free and trapped) as a function of the excitation intensity using eq 2. It is worth pointing out that a possible underestimation of the effective charge density can be due to the overlap between the dye bleaching band and the tail of its oxidized species absorption band. However, this effect is a systematic error which should not depend on excitation intensity or temperature. Figure 2b shows a typical photoconductivity trace which is used to extract the electron mobility. The photovoltage is read directly from the oscilloscope, from which the photoconductivity can be calculated using eq 3.

Figure 3a shows the mobility as a function of the total charge density at temperatures from 110 to 295 K. Several general trends are present over the investigated temperature range. First, the charge density dependence is shown to be only slight at low temperatures (≤170 K) and gradually increases as the temperature is raised above 170 K. Taking a concentration of $n = 3.2 \times 10^{17}$ cm^{-3}, where we have mobility measurements for all temperatures, we see that the mobility rises with temperature from 110 to 260 K and then falls with increasing temperature when it is raised beyond 260 K. This behavior is not what one would expect, since electron transport is usually described by
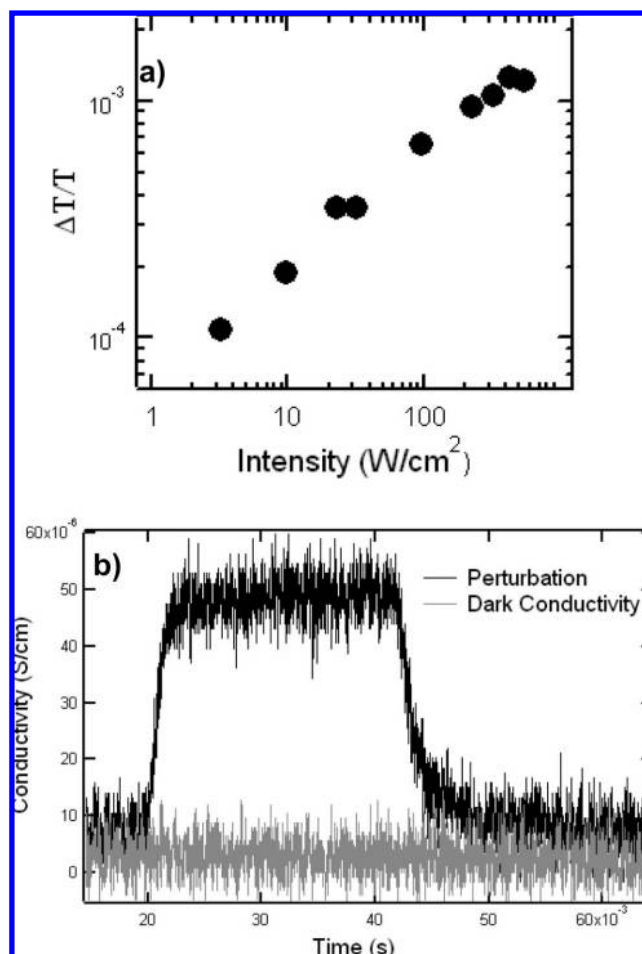

Figure 2. (a) PIA signal ($r = \sqrt{(x^2 + y^2)}$) at 560 nm plotted as a function of the pump intensity modulated at 23 Hz. Here, the device structure is the same as the one shown in Figure 1a. (b) Photoconductivity (black line) measured simultaneously with the PIA signal by an oscilloscope triggered at the laser pump modulation frequency (23 Hz). The dark conductivity (gray line) is also shown. The marginal discrepancy between the bottom of the "photoconductivity" trace and the dark conductivity is due to the sample not fully relaxing during the cycle.

a thermally activated MT model. We note here, however, that Hendry et al. also observe an increase in the conductivity in both single-crystal and mesoporous TiO₂, as studied by terahertz spectroscopy, as the temperature is reduced from room temperature to 100 K.[15]

In order to confirm the validity of these data, we performed an analysis of experimental artifacts which may affect the results obtained, and we have also repeated the measurements many times on various samples. As explained above, our calculated mobility data are corrected for a "background" charge density arising from species longer lived than the modulation frequency. We tested the effect of the background correction by recalculating and replotting the data taking the modulated photoinduced charge density as the total charge density. There are some small deviations in the curves compared to the corresponding background-corrected curves in Figure 3a; however, the same trends with temperature and charge density are still observed. In Figure 3b we show extracted data at a charge density of 3.2×10^{17} cm^{-3} for the "raw" perturbation mobility (corresponding to no

(13) Moser, J. E.; Noukakis, D.; Bach, U.; Tachibana, Y.; Klug, D. R.; Durrant, J.; Humphry-Baker, R.; Grätzel, M. *J. Phys. Chem. B* **1998**, *102*, 3649.

(14) Tachibana, Y.; Moser, J. E.; Gratzel, M.; Klug, D. R.; Durrant, J. R. *J. Phys. Chem.* **1996**, *100*, 20056.

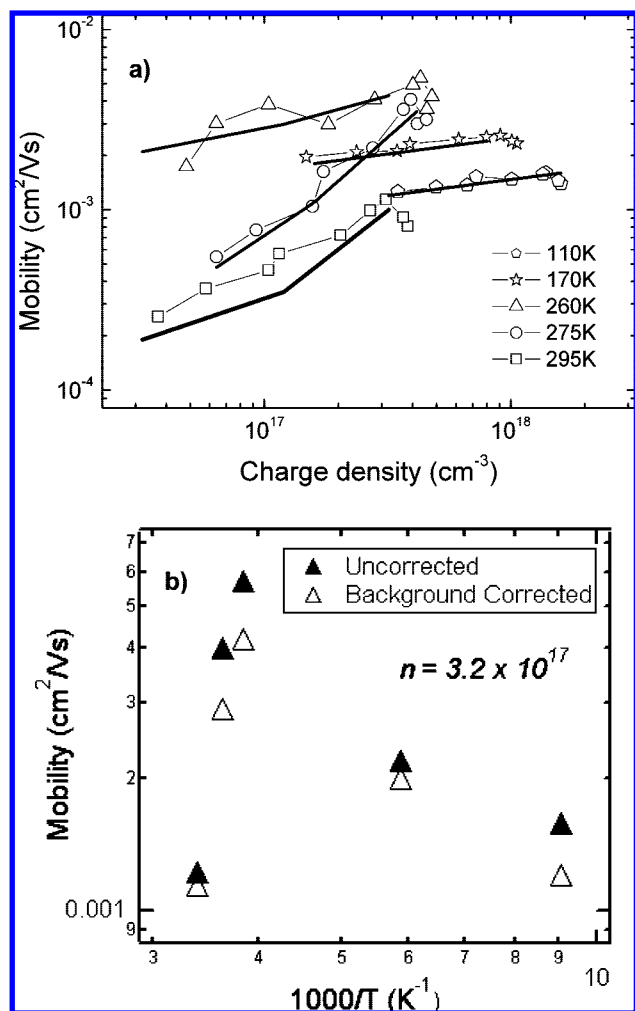(15) Hendry, E.; Koeberg, M.; O'Regan, B.; Bonn, M. *Nano Lett.* **2006**, *6*, 755.

Figure 3. (a) Electron mobility plotted at various temperatures as a function of the total charge density present in the device. Here, the mobility has been calculated from the total photoconductivity which also takes into account the steady-state background "photoconductivity" component and the total charge density (background-corrected). The symbols, connected by faint lines, represent the experimental data, while the heavy lines are MT Monte Carlo fits at temperatures between 110 and 295 K. (b) Temperature dependence of the mobility at a fixed total charge density of 3.2×10^{17} cm^{-3} for the mobility extracted from panel a and also for the mobility estimated without taking into account the background charge density. For the latter the mobility was calculated from the simple relation $\mu = \Delta\sigma/ne$, where μ is the electron mobility and $\Delta\sigma$ is the change in photoconductivity measured through the oscilloscope; see text. This has been done to consider to what extent the mobility trend over different temperatures is affected by charge species longer lived than the modulation frequency.

background correction) and that corrected for the increasing background (corresponding to the data from Figure 3a) as a function of $1000/T$. The uncorrected mobility is slightly higher as expected, but the trend remains.

Electron–Hole Recombination. Further to probing the charge transport, we can also derive information about the recombination kinetics from the transient photoconductivity measurements. From our combined measurements we know the time-dependent conductivity and we also know the charge-density-dependent conductivity. Therefore, by compiling thes data we can extract the time-dependent charge density. An example of the transient electron density trace is shown in Figure 4a. These data are optimally fitted by a stretched-exponential function: $n(t) = K$
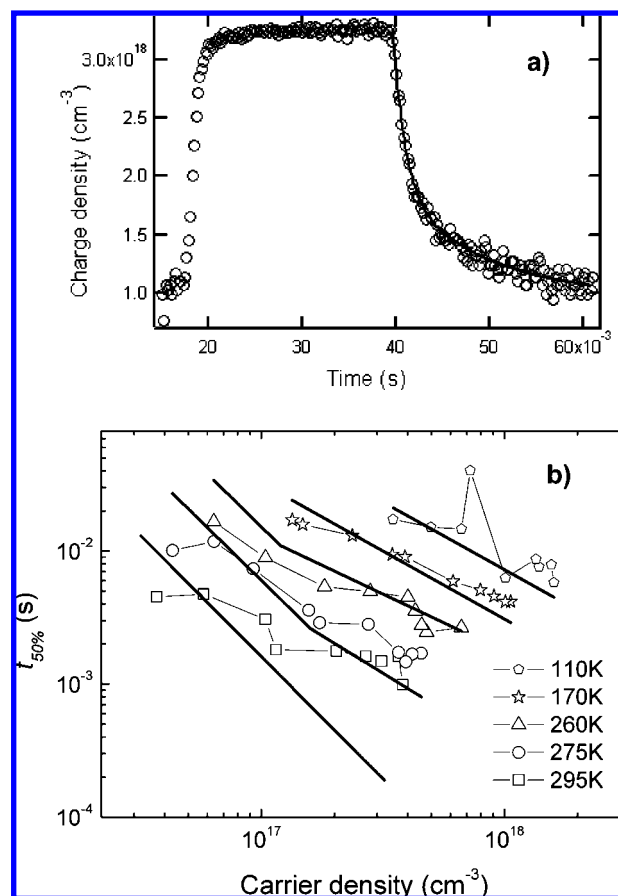

Figure 4. (a) Example of a transient charge density trace $n(t)$, derived from the time dependence and charge density dependence of the conductivity. The time-dependent photoconductivity ($\sigma(t)$) is directly measured, and the "time-dependent charge density" ($n(t)$) is estimated from $\sigma(t)$ knowing $\sigma(n)$. The charge density decay has been fitted by a stretched-exponential function. (b) Electron half-life ($t_{50\%}$) plotted (symbols connected by faint lines) as a function of the total charge density in the same temperature range explored for the mobility studies (from 110 to 295 K). MT Monte Carlo predictions (heavy lines) of electron half-life, $t_{50\%}$, are also shown.

$\exp(-(t/\tau)^\alpha)$ (shown), from which we can obtain the electron half-life, $t_{50\%}$. In Figure 4b we show $t_{50\%}$ as a function of the total charge density and temperature.

Discussion of Experimental Results

Electron transport in mesoporous TiO$_2$ is mediated by traps within the material that reduce the mobility below the 1 cm^2/V·s measured for single crystals.[15] Typically, transport in TiO$_2$ is described by either MT[16−19] or thermally assisted hopping,[16,20] with MT being preferred since it gives better fits to experimental data.[16] However, both of these models are, to some extent, thermally activated and so in their original form cannot describe the peak in mobility when $T = 260$ K.

There is little precedent as to why the mobility might vary in this manner with temperature; indeed, to the authors'

(16) Nelson, J.; Haque, S. A.; Kluh, D. R.; Durrant, J. R. *Phys. Rev. B* **2001**, *63*, 205321.
(17) Anta, J. A.; Nelson, J.; Quirke, N. *Phys. Rev. B* **2002**, *65*, 125324.
(18) Anta, J. A.; Mora-Sreo, I.; Dittrich, T.; Bisquert, J. *J. Phys. Chem. C* **2007**, *111*, 13997.
(19) Nelson, J. *Phys. Rev. B* **1999**, *59*, 15374.
(20) Bisquert, J. *J. Phys. Chem. C* **2007**, *111*, 17163.
(21) Mott N. F.; Davis E. A. *Electronic processes in non-crystalline materials*; Clarendon Press: Oxford, England, 1971.

knowledge there is only one explicit mechanism reported that may explain this type of behavior. In ref 21 it is described how, when raising the temperature, a polaron may dissociate and begin to experience band-like transport. Hence, at low temperatures, transport of the polaron would be assisted by thermal energy, and at high temperatures, the transport of the free carrier would be hindered by thermal energy via phonon scattering. While this explanation could qualitatively explain the trend seen in Figure 3b, it is generally not consistent with the concentration dependence of mobility shown in Figure 3a. For instance, at low temperatures, where this physical picture would imply the formation of a polaron, we find little concentration dependence of mobility, counter to what would be expected. Further, at high temperatures, where this physical picture would predict band-like transport, we find a very strong concentration dependence of mobility which is again counter to what would be expected. In any case, the number of investigations which find close agreement between various transport phenomena in TiO₂ and MT models[16-19] makes it seem unlikely that all of the present data could be explained by replacing the MT transport mechanism.

Qualitatively, one can conceive that the present data could be recreated within the MT model if the DoS became less deep with reducing temperature. Such a suggestion has been made for TiO₂ in a number of previous investigations. Anta et al.[18] found that in order to fit a Monte Carlo model to surface photovoltage transients, the mean depth of the exponential DoS, E_0, had to drop from 60 meV at 300 K to 47 meV at 150 K. Further, temperature-dependent capacitance−voltage data[22] for 10 nm TiO₂ particles were interpreted as a reduction in E_0 from 100 meV at 320 K to 80 meV at 280 K. This change in the DoS was attributed to charged particles within the pores of the film, which we can consider to be due to defect sites such as Ti_3^+, protons from the dye, or impurities. These charged particles contribute a Coulombic term to the trap energy, and since the dielectric displacement, $D = \varepsilon F$ (where F is the electric field), is constant over the air−TiO₂ interface, the magnitude of the Coulombic term varies with temperature due to the temperature dependence of the dielectric constant of TiO₂, ε_R.[23] We do note, however, that this mechanism was proposed for 10 nm TiO₂ particles, and it is not known whether this effect would be as important in the current 20 nm sized particles.

Since traps in TiO₂ are due to many and varied factors (for example, the crystal structure and defects therein, both at the surface and in the bulk, the degree of protonation, chemical impurities, and so on), it is possible that there may be other reasons why the DoS may change with temperature. We view determining the cause of a change in the DoS with temperature to be outside the scope of the current investigation. However, we are sufficiently encouraged by the present data, along with other transport-based[18] and non transport-based[22] studies, to consider that it is likely that the DoS does change with temperature. Hence, we shall now characterize the current data using a MT Monte Carlo model in which the DoS is allowed to vary with temperature.

Monte Carlo Modeling

Model Development. The MT model was originally proposed by Scher and Montroll[24] and later used for TiO₂ by a number of authors.[16-19] In many of these models[16-18] the electric field,

$\bar{F}$, is either neglected or absent and so they consider only diffusion. The question of how to model carrier drift using MT is not straightforward. In ref 17, the energy barrier to detrapping is modified by an amount, $\bar{F}a\bar{u}_{i\rightarrow j}/2$, where a is the intertrap distance and $\bar{u}_{i\rightarrow j}$ is the unit vector pointing from the occupied trap to the destination trap. However, we found that applying this technique did not provide sufficient driving force downfield to yield the experimentally derived mobilities. Hence, following Scher and Montroll,[24] we decouple the detrapping process from the subsequent net motion of the carrier downfield. In this case, the distribution of detrapping times is generated from

$$t_{i\rightarrow j} = -\ln(r)t_0 \exp(E_i/kT) \qquad (4)$$

Here, t_0 is a characteristic detrapping time, r is a randomly distributed number between 0 and 1, and E_i is the energy of the occupied trap. Note that $E = 0$ corresponds to the high-mobility band edge and that energy here becomes more positive as we move from the high-mobility band edge into the bandgap. We make the common assumptions that traps are regularly spaced at intervals a in each of the Cartesian directions and that detrapped carriers can only move to a nearest-neighbor trap. The motion of carriers once they have detrapped to the high-mobility state is described by an angular velocity distribution which has an isotropic (diffusive) component and a small anisotropic (drift) component which is proportional to the electric field. This is analogous to the assumption made by Scher and Montrol[24] to fit to time-of-flight data in highly dispersive As₂Se₃, and in other situations where carriers undergo strong phonon scattering.[25] The probability of a detrapped carrier moving into an adjacent cell j is thus

$$p(i\rightarrow j) = \frac{1}{6} + C\bar{u}_{i\rightarrow j}\bar{F} \qquad (5)$$

where C is a constant that describes the anisotropic (drift) part of the velocity distribution. Implicit in this model is the assumption that the carrier is trapped for a much longer time than it is free. We choose $a = 2$ nm, as this corresponds to the middle of the measured trap concentrations in TiO₂,[26] and $t_0 = 5 \times 10^{-13}$ s, since this has been shown to adequately describe diffusion in the absence of recombination in previous MT models.[17] Mobility is fitted via C and the chosen probability density function for the DoS, $p(E)$. Throughout this paper we use exponential, $p(E) = a \exp(-E/E_0)$, and Gaussian, $p(E) = a \exp(-(E - E_0)^2/2\sigma^2)$, DoS functions, where a is a constant chosen to give unity probability over the range of $p(E)$ (which is 0 to $+\infty$ unless otherwise stated) and E_0 is the characteristic center of the DoS function.

In the limit of strong scattering, the perturbation caused by the electric field upon the velocity distribution is small.[20] Hence we choose $C = 10^{-6}$, as this is the lowest value which gives mobilities of the order seen in experiment using sensible values for the remaining fit parameters. We note that we found it impossible to fit the experimental data using larger values of C, perhaps suggesting some degree of uniqueness to the fit parameters used. In order to limit the number of fitting parameters available, we do not distinguish between surface or bulk states nor take into account film porosity. The simulation volume extends 50 trap states in each Cartesian direction and has circular boundary conditions for computational efficiency,

(22) Abayev, I.; Zaban, A.; Kytin, V. G.; Danilin, A. A.; Garcia-Belmonte, G.; Bisquert, J. *J. Solid State Electrochem.* **2007**, *11*, 647.

(23) Parker, R. *Phys. Rev.* **1961**, *124*, 1719.

(24) Scher, H.; Montroll, E. W. *Phys Rev. B* **1975**, *12*, 2455.

(25) Wolff, P. A. *Phys. Rev.* **1954**, *95*, 1415.

(26) Fabregat-Santiago, F.; Mora-Sero, I.; Garcia-Belmonte, G.; Bisquert, J. *J. Phys. Chem. B* **2003**, *107*, 758.

although tests were performed to ensure that the finite size of the simulation volume did not affect the results obtained. Due to the large dielectric constant of TiO_2 ($\varepsilon_R \approx 100^{23}$) we do not include carrier-carrier Coulomb interactions, other than disallowing double occupancy of a trap.

To simulate mobility, carriers are injected at random positions throughout the simulation volume. For each carrier a detrapping time is calculated using eq 4, and a retrapping destination determined using eq 5. The field for all simulations was 1.5×10^4 V/m, as in the experiment. The electron with the shortest wait time is moved, and the waiting times for the remaining detrapping events are shortened by the corresponding amount before a new behavior for the moved carrier is determined. As high carrier densities are being considered, a dynamical Monte Carlo implementation is used in which the behavior of carriers is recalculated if their destination trap becomes filled. Successive detrapping events are performed until the simulation terminates. At 2.5 ms intervals, the average distance moved downfield by the ensemble of carriers is recorded to determine the mobility. In this way the mobility as a function of time is determined, so that we can be sure we are measuring the average mobility and not transient-enhanced mobility arising from carriers being injected with a nonequilibrium energy distribution. Each simulation runs until the simulation time reaches 10 ms. Mobilities determined by this technique show deviation between trials of only $\sim 5-10\%$.

We also examine the recombination kinetics by fitting a slightly modified version of the Monte Carlo model just described to the experimental $t_{50\%}$ data shown in Figure 4. For these simulations, a randomly placed immobile cation was injected for each electron. The assumption of randomly distributed electrons and cations may be a source of error in our modeled data. However, since these films are much thinner than the optical depth of the composite, we do expect reasonably uniform light absorption throughout the film. Electrons are allowed to recombine with adjacent cations only, at a rate k_s, which competes with the rate of detrapping. Electrons are disallowed from drifting or diffusing into the cation site via the high-mobility state. This is in order to prevent "barrier-free" recombination which is unlikely since the recombination reaction is usually considered to proceed via a Marcus charge-transfer-like process.[27] Recombining electrons and holes are removed from the simulation until half of the cations have been lost, at which point $t_{50\%}$ is recorded and the simulation repeated many times to ensure sampling of average behavior. The recombination rate constant, k_s, is allowed to vary to fit the data; otherwise, all other fitting parameters and DoS functions are as determined during mobility simulations.

Modeling Results. The choice of DoS function for use in MT models is not straightforward since it is ultimately a mathematical convenience that may bear only broad similarities with the true DoS, which itself can only be approximately measured. This is compounded by the strong sensitivity of the mobility and its charge density dependence to subtle changes in the lower lying trap states, as reported by Anta et al.[17] and also found to be the case for the current work. We are therefore left with the awkward situation of being constrained to mathematical functions for the DoS that may not have any particular physical significance, even though it is known that subtle changes in the DoS can cause large changes in the predicted mobility. We would therefore like to underline that although our DoS

Table 1. Parameters Used in the Simulation[a]

	Gaussian			exponential	
	110 K	170 K	260 K	275 K	295 K
E_0, meV	85	143	30	52	59
σ, meV	20	20	100	n/a	n/a
k_s, s^{-1}	6×10^4	8×10^4	3×10^7	4×10^7	10^{10}
$\langle E \rangle$, meV	126	170	352	450	500

[a] For the Gaussian DoS functions, E_0 denotes the center of the function, whereas for the exponential DoS functions, E_0 denotes the average trap depth. σ is the standard deviation of the Gaussian DoS distribution. k_s is the recombination rate of adjacent electrons and cations. $\langle E \rangle$ is the average occupied trap energy for a charge density of $n = 3.2 \times 10^{17}$ cm^{-3}.

functions are necessarily precise to fit the data, we do not view the true DoS to be exactly as reported. There is, however, physical meaning in the general trend of the DoS functions, and so we shall infer broad generalities from the functional form of the DoS as the temperature is changed.

For $T = 295$ and 275 K, it was found that an exponential DoS gave too great a charge density dependence and that a broad Gaussian DoS gave too little a charge density dependence. It was only possible to fit the current data by choosing an exponential of mean depth $E_0 = 59$ and 52 meV for 295 and 275 K, respectively, which excluded the DoS lying 600 meV below the high-mobility band edge in a manner similar to that reported by Anta et al.[17] Even though part of the DoS is excluded for these temperatures, the charge density dependence of mobility still shows the power law dependence seen in experiment. An exponential DoS was found to give too great a concentration dependence for the data where $T \leq 260$ K. This implies that the DoS for $T \leq 260$ K is narrower than an exponential, and so instead a Gaussian DoS is used in which the standard deviation, σ, is used to fit the concentration dependence and E_0 to fit the magnitude of the mobility. The DoS functions determined by fitting are shown in Table 1. For $T = 260$ K the Gaussian function used includes a component with energies greater than the high-mobility state, and in these cases the energy is reduced to the high-mobility state energy, $E = 0$. In practice this small modification makes little difference to the results obtained, as it is the deepest states that primarily determine the mobility. Figure 3a shows the modeled data together with the experimental mobility data.

It can be seen that good fits to the mobility were achieved for all temperatures. As discussed previously, the DoS functions chosen are mathematical conveniences, and so to probe the average trap depth we do not consider the DoS function but rather the more physically meaningful time-averaged occupied trap energy, $\langle E \rangle$, which is shown in Table 1. In qualitative agreement with what has been found by Anta et al.[18] and Abayev et al.,[22] we find that, in order to fit the data, the average occupied trap depth increases with increasing temperature. We note that for the Gaussian DoS functions $\langle E \rangle$ agrees well with the analytical formula for equilibrium energy in a Gaussian disordered system reported by Bässler[28] ($\langle E \rangle = E_0 + \sigma^2/kT$ relative to the band-edge). When the DoS is exponential $\langle E \rangle$ is the Fermi level. The DoS functions are found generally to broaden as the temperature increases, since the values of σ for the Gaussian DoS, and E_0 for the exponential DoS, tend to increase with temperature. The fitted DoS functions are also in accordance with a broadening of the DoS as temperature

(27) Moser, J. E.; Grätzel, M. *Chem. Phys.* **1993**, *176*, 493.

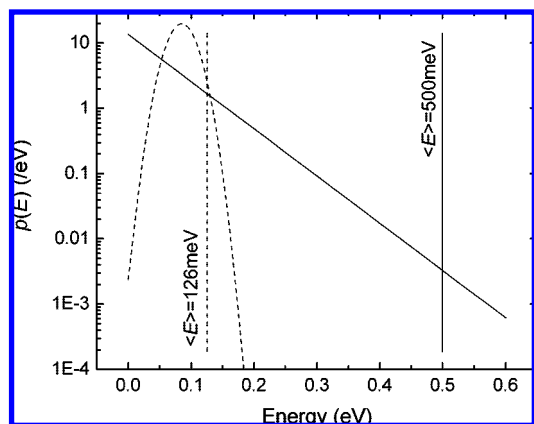(28) Bässler, H. *Phys. Stat. Sol. (b)* **1993**, *175*, 15.

Figure 5. DoS functions determined by Monte Carlo fitting when $T = 295$ K (solid curve) and 110 K (dashed curve). Vertical lines denote the average carrier energy $\langle E \rangle$ for the corresponding temperature at a concentration of 3.2×10^{17} cm^{-3}.
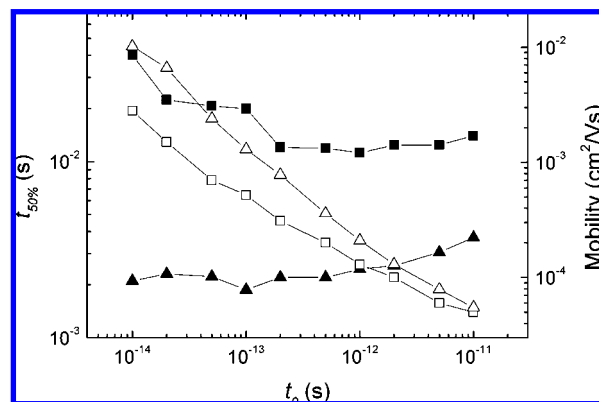

Figure 6. Electron half-life, $t_{50\%}$ (filled symbols), and mobility (open symbols) as predicted by MT Monte Carlo simulations as a function of the detrapping rate prefactor, t_0 when $T = 295$ K and the charge density is 3.2×10^{16} (squares) or 1.3×10^{17} cm^{-3} (triangles). All other parameters were held constant and as used for modeling the experimental data.

increases, since the Gaussian DoS used at low temperature decays as $\sim\exp[-(E/\sigma)^2]$ as opposed to an exponential DoS which decays as $\sim\exp[-(E/E_0)]$. This can be seen more easily in Figure 5, where we show the DoS functions for $T = 295$ and 110 K together with the average occupied trap energy $\langle E \rangle$ at a concentration of 3.2×10^{17} cm^{-3}.

It is worth reiterating at this point the difficulty of fitting with this simple model to a mobility data set that extends over both temperature and carrier concentration. It was not possible to achieve good fits while keeping the form of DoS constant over temperature, nor was it possible to fit the data when C (a constant that describes the anisotropic (drift) part of the velocity distribution) was varied considerably. A hopping model was also tested but found to be unable to fit the current data. Hence, if one interprets electron transport in TiO₂ in terms of a simple, homogeneous MT model,[16−19] we are confident that the only way one can explain all the current data within this framework is via the DoS becoming shallower and narrower as the temperature falls.

Good fits to recombination data were also achieved, shown in Figure 4b, using k_s as the only fit parameter, the values of which are shown in Table 1. In agreement with Moser et al.,[13] we found that the recombination rate had to be large in order to achieve good fits to data. The positive temperature dependence of k_s is indicative of recombination being an activated process, perhaps due to the electronic reorganization of the dye complex upon absorption of the electron. The poor fit to $t_{50\%}$ at high concentrations when $T = 295$ K should be ignored since these time values are close to the temporal resolution limit our measurement system. The concentration dependence of $t_{50\%}$ for 110 and 170 K is primarily due to the bimolecular nature of the recombination process, since the concentration dependence of mobility is very small. As the concentration dependence of mobility increases with temperature, the concentration dependence of $t_{50\%}$ also increases marginally. To clarify what is meant by bimolecular effects: The rate at which the recombination reaction will occur is proportional to the density of the electrons and holes taking part in the reaction, n and p, and the transport-related Langevin coefficient. Here $n = p$ by the nature of electron injection, and hence recombination increases quickly as n^2.

Probing the Transport and Recombination Regime. It is of technological interest to ask the question what limits the degree

of recombination at room temperature (295 K). In principle there are two regimes for recombination: one, when the detrapping rate is much faster than the recombination rate, and the other, vice versa. In the first instance, when an electron finds itself adjacent to a cation, it has a very good chance of detrapping before recombining, and hence the overall charge lifetime is directly influenced by the recombination rate constant. This is often inelegantly termed recombination-limited recombination. In the second instance, once an electron has found a site adjacent to a cation, it will usually recombine before it detraps, and in this instance the overall charge lifetime is limited by the rate of arrival of electrons to the cation sites. This is usually termed transport- or diffusion-limited recombination. To probe this experimentally is highly challenging since uniquely altering individual parameters is close to impossible. Here, however, we take advantage of our numerical approach and attempt to clarify this issue for this system by predicting the electron half-life when $T = 295$ K (and all other parameters as described previously) for a range of detrapping prefactor, t_0, when the charge density is 3.2×10^{16} or 1.3×10^{17} cm^{-3}. This is shown in Figure 6 along with the predicted electron mobility. We note that t_0 is not the detrapping time but the prefactor in eq 4 which is proportional to the detrapping time. For comparison, the value of 5×10^{-13} s was used for fitting the experimental data, in the middle of the range investigated here. As expected, the mobility increases almost linearly with decreasing prefactor for both charge densities, with the higher charge density showing a greater slope.

First looking at $t_{50\%}$ for the lower charge density (Figure 6, top curve), it can be seen that when t_0 decreases below 0.2 ps the electron half-life increases. This can be attributed to the competition between recombination and increasingly efficient detrapping; i.e., once an electron finds a cation it is increasingly likely to detrap before recombining. When 0.2 ps $\geq t_0 \geq$ 2 ps, the electron half-life is almost constant. This suggests that electrons are finding cations to recombine with sufficiently quickly, and that instead recombination is limited by the recombination rate. A slight rise in electron half-life occurs when t_0 increases beyond 2 ps, showing that increasingly inefficient transport is slowing the recombination process, i.e., transport-limited recombination. Investigating the regime $t_0 > 2$ ps is computationally demanding; however, an isolated test point for $t_0 = 200$ ps confirms that the recombination half-life continues

to increase. Hence, the model predicts, for the parameters used to fit the experimental data, that recombination is limited by the recombination rate and not by transport.

The corresponding curve for the higher charge density (Figure 6, bottom curve) shows that the electron half-life is very much smaller, despite the small change in mobility, showing that bimolecular effects play a dominant role in determining the variation of recombination with varying charge densities. The shape of the curve for the higher charge density is similar to that at low charge density, for the same mechanisms as discussed previously, but displays a smaller variation of half-life upon reducing the prefactor below 0.2 ps, but a larger variation upon increasing the prefactor above 1 ps. Computational resources prohibited a thorough investigation of the half-life outside the range 10 fs $\geq t_0 \geq$ 10 ps. However, tests of half-life as t_0 increases outside this range confirmed that the half-life continued to increase in both directions. The reason for the weaker dependence of half-life upon the prefactor reduction is as follows. When the charge density increases, so does the probability of having an electron adjacent to a cation. Consequently, as there is a more ready supply of electrons and cations that can undergo recombination at any given time, the half-life displays a weaker dependence on increasingly rapid detrapping. Since the increase in $t_{50\%}$ with increasing t_0 above 1 ps is consistent with diffusion-limited recombination, the slightly steep rise for the high charge density regime is likely to be contributed by the more steeply varying mobility.

To summarize this last investigative section, according to our model the main factor determining the charge density dependence of the recombination at room temperature is not the increase in mobility, but the increased charge density and the bimolecular nature of the recombination. At room temperature, the system appears to have made a transition from transport-limited recombination to recombination-limited recombination at both high and low charge densities. Though this appears to be convincing, we must stress that these findings are an interpretation of this model, and the model is based on the various assumptions described above. However, it does imply that if the trap depth can be reduced, or the mobility enhanced

without increasing the charge density, then significant improvements in transport without detrimentally influencing the recombination are possible.

Conclusions

In summary, we have observed the charge density and temperature dependence of the mobility in TiO_2 to be such that, at high temperatures, there exists a strong charge density dependence which diminishes with reducing temperatures, and at temperatures below 260 K the mobility appears to be almost independent of charge density. The general trend with temperature is such that the mobility at first increases and then decreases with reducing temperature at any given charge density. It is only possible to fit our observations with a multiple-trapping model for charge transport if we allow the average trap depth to become deeper and the density of states to become more disordered as the temperature is increased. As mentioned above, this is actually rather likely. Modifying the charge-transport model to allow recombination with cations, our observed recombination kinetics are also consistent with the above-mentioned variation in density of states. In contrast to the peculiar trend observed for transport data, the recombination half-life ($t_{50\%}$) monotonically decreases with increasing charge density and temperature. The charge density dependence of the recombination at low temperatures arises almost entirely from the bimolecular nature of the process (rate $\propto n \times p$). Our analysis also suggests that at room temperature the recombination is weakly influenced by the charge transport and mainly influenced by the recombination reaction and the cation density.